EuroIntervention 2019;15:902-911

# Impact of abrupt versus gradual correction of mitral and tricuspid regurgitation: a modelling study

**John Walmsley**[1], PhD; Pierre Squara[2], MD; Ulrich Wolfhard[3], MD; Richard Cornelussen[4], PhD; Joost Lumens[1,5]*, PhD

*1. CARIM School for Cardiovascular Diseases, Maastricht University Medical Center, Maastricht, the Netherlands; 2. Department of Critical Care Medicine, CMC Ambroise Paré, Neuilly-sur-Seine, France; 3. Medtronic GmbH, Meerbusch, Germany; 4. Bakken Research Center, Medtronic plc, Maastricht, the Netherlands; 5. L'Institut de Rythmologie et Modélisation Cardiaque (IHU-LIRYC), Université de Bordeaux, Pessac, France*

*This paper also includes supplementary data published online at: https://eurointervention.pcronline.com/doi/10.4244/EIJ-D-19-00598*

**KEYWORDS**

- innovation
- mitral regurgitation
- preclinical research
- specific closure device/technique
- tricuspid disease

## Abstract

**Aims:** Correction of mitral and/or tricuspid regurgitation (MR, TR) frequently leads to poor outcomes in the days following intervention. We sought to understand how abrupt correction of MR and TR affects ventricular load and to investigate if gradual correction is beneficial.

**Methods and results:** MR and TR were simulated using the CircAdapt cardiovascular system model with effective regurgitant orifice (ERO) areas of 0.5 $cm^2$ and 0.7 $cm^2$. Ventricular and atrial contractility reductions to 40% of normal and pulmonary hypertension were simulated. Abrupt and gradual ERO closure were simulated with homeostatic regulation of blood pressure and volume. Abrupt correction of MR increased left and right ventricular fibre stress by 40% and 15%, respectively, whereas TR correction increased left and right ventricular fibre stress by 26% and 19%, respectively. This spike was followed by a rapid drop in fibre stress. Myocardial dysfunction prolonged the spike but reduced its amplitude. Right ventricular fibre stress increased more with pulmonary hypertension and TR. Gradual correction demonstrated no spike in tissue load.

**Conclusions:** Simulations demonstrated that abrupt ERO closure creates a transient increase in ventricular load that is prolonged by worsened myocardial condition and exacerbated by pulmonary hypertension. Gradual closure of the ERO abolishes this spike and merits clinical investigation.

**Corresponding author: Dept. Biomedical Engineering (UNS50, room H3.362), CARIM School for Cardiovascular Diseases, Maastricht University Medical Center, PO Box 616, 6200 MD Maastricht, the Netherlands. E-mail: joost.lumens@maastrichtuniversity.nl*



SUBMITTED ON 25/06/2019 - REVISION RECEIVED ON 21/08/2019 - ACCEPTED ON 10/09/2019

DOI: 10.4244/EIJ-D-19-00598

EuroIntervention 2019;15:902-911

## Abbreviations

| | |
|---|---|
| **CO** | cardiac output |
| **EF** | ejection fraction |
| **ERO** | effective regurgitant orifice |
| **LA** | left atrium |
| **LV** | left ventricular |
| **MAP** | mean arterial pressure |
| **MR** | mitral regurgitation |
| **PH** | pulmonary hypertension |
| **RA** | right atrium |
| **RV** | right ventricular |
| **TR** | tricuspid regurgitation |

## Introduction

Chronic mitral regurgitation (MR) and tricuspid regurgitation (TR) cause progressive ventricular and atrial enlargement through altered protein expression, sarcomere remodelling, and myocyte elongation that creates a "vicious cycle" of dilatation and worsening regurgitation[1-4]. Due to compensatory remodelling, patients are frequently asymptomatic[5]. When indicated, repair or replacement of the valve aims to restore competency, abruptly terminating retrograde flow[6]. If indicated, tricuspid valve repair or replacement is generally performed concomitant with left-sided valve intervention[7]. Long-term residual regurgitation due to incomplete repair or paravalvular leakage allows the cycle of dilatation and regurgitation to restart and is associated with worse long-term outcomes[8,9].

Patients undergoing mitral valve replacement for chronic regurgitation experience longer stays in intensive care including extracorporeal life support, use of inotropes, and mechanical ventilation than for other cardiac interventions at similar levels of risk such as aortic valve replacement[10,11]. In-hospital mortality from mitral valve replacement surgery has recently been reported at 5.5% with 63.3% morbidity[12]. We hypothesised that abrupt changes in ventricular loading conditions in patients with chronic regurgitation following valve replacement may be harmful in the short term and contribute to post-procedural myocardial dysfunction and mortality. We additionally hypothesised that gradual correction of regurgitation may be beneficial by gently unloading the heart while fully resolving regurgitation. A proposed modification to prosthetic valves to allow gradual correction is shown in **Figure 1**. To investigate these hypotheses in a controlled manner, we simulated correction of MR and TR in a validated cardiovascular system model and compared the effects of abrupt and gradual correction of regurgitation on cardiac pump function and tissue mechanics.

## Methods

### THE CIRCADAPT MODEL

CircAdapt is a well-established lumped-parameter model of the heart and circulation that enables realistic simulation of beat-to-beat cardiovascular mechanics and haemodynamics **(Figure 2A)**[13-15]. Valvular flows in health and disease have been validated through direct comparison both with clinical Doppler recordings and with derived echocardiographic parameters[14,16]. Ventricular tissue mechanics and pump function have been extensively and quantitatively validated against experimental and clinical measurements, including myocardial strain from tagged magnetic resonance data and echocardiography[15,17,18]. Furthermore, CircAdapt enables simulation of myocardial structural adaptation to chronic alterations in mechanical load due to exercise training or pathology[19]. Adaptation alters the thickness, area, and stiffness of heart and blood vessel walls in the systemic and pulmonary circulations to normalise local tissue loading. All simulations in this paper use source code downloadable from www.circadapt.org[15]. Detailed descriptions of the modules below are provided in **Supplementary Appendix 1**. A simulation flow chart is shown in **Supplementary Figure 1**.

### HOMEOSTATIC CONTROL

Circulating blood volume is used to maintain mean arterial pressure (MAP) and cardiac output (CO) through homeostatic control, representing venous pooling and fluid retention or excretion by the renin-angiotensin-aldosterone system. When homeostatic control is enabled, the ratio of the current MAP to the target MAP is calculated after each simulation of a single cardiac cycle, as is

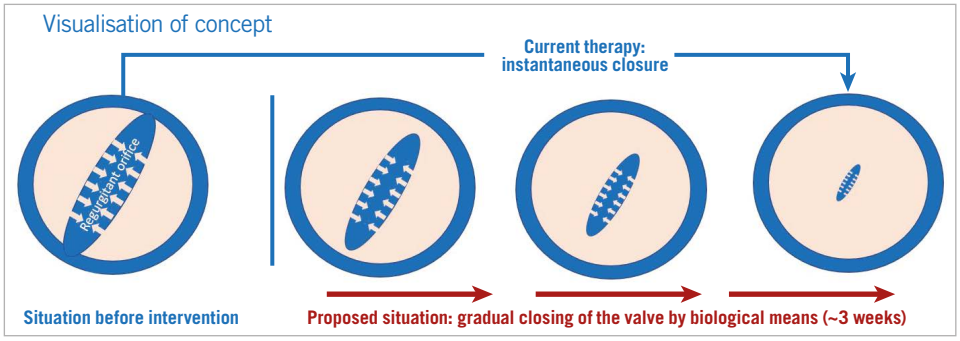


**Figure 1.** *Gradual reduction of regurgitation. We envisage a transiently leaking prosthetic valve with the following characteristics. The valve would admit a regurgitant flow on implantation. Over the following weeks, the regurgitation diminishes until complete closure is achieved through a degrading biogel on the valve leaflets that impedes closure.*

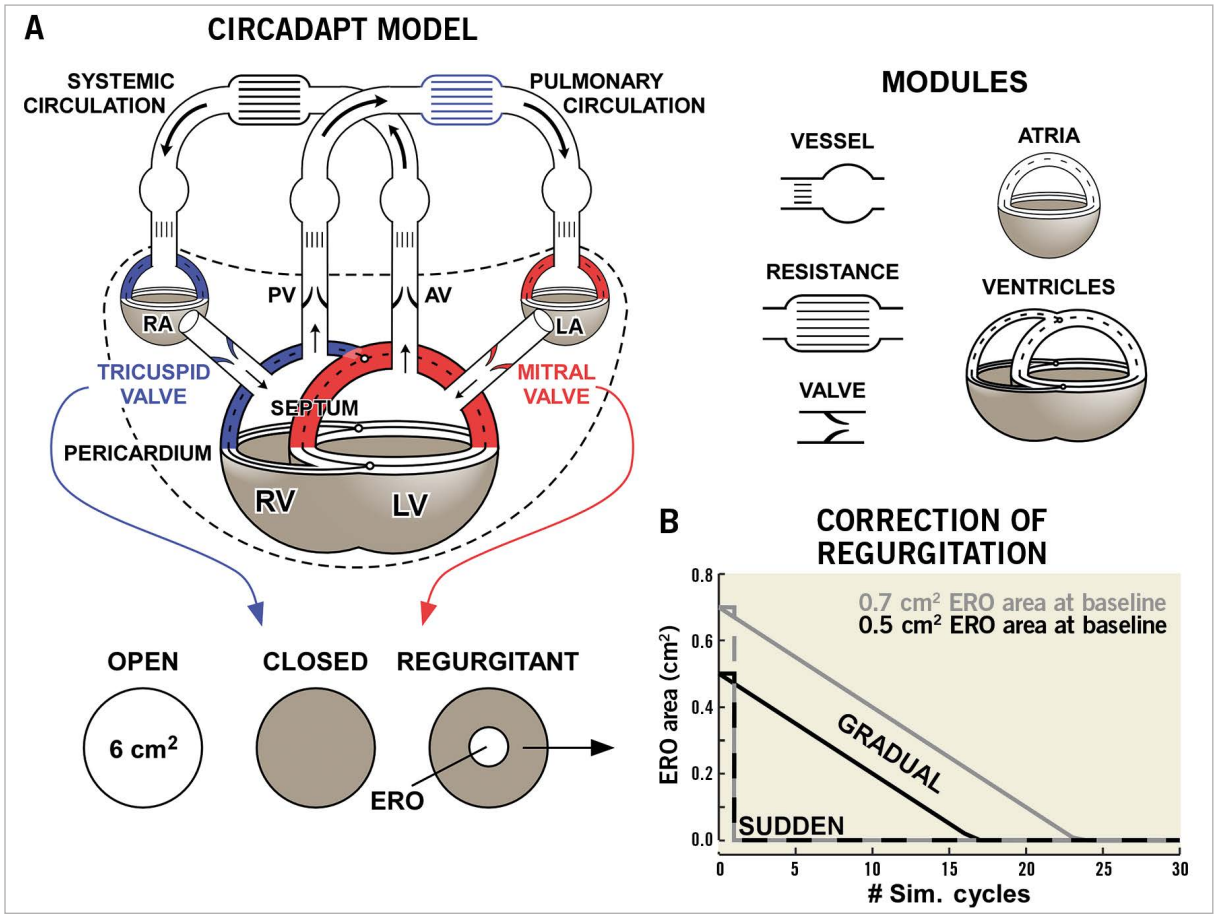


**Figure 2.** *Computational methods. A) The structure of the CircAdapt cardiovascular system model. The left ventricle (LV), left atrium (LA), and mitral valve are highlighted in red. The right ventricle (RV), right atrium (RA), tricuspid valve, and pulmonary circulation are highlighted in blue. Modified from Lumens et al with permission[14]. B) The course of closure of a valve ERO area of 0.5 cm² (black) and 0.7 cm² (grey) for sudden closure (dashed lines) and gradual closure (solid lines).*

the ratio of the current CO to the target CO. Systemic vascular resistance increases when MAP is too low and decreases when CO is too low, mimicking systemic arteriolar constriction or dilation. Blood is injected or removed from the systemic circulation based on the ratio of MAP. Subsequent simulation cycles repeat this process until the target MAP and CO are reached. Each cycle with homeostatic control enabled represents a snapshot into a process that takes hours to days, and that depends on renal function amongst other factors.

### VALVULAR FUNCTION

The valve module simulates blood flow between two cardiac chambers, or a chamber and a large vessel, where energy losses can occur. The valve is a narrow orifice whose area varies over time during a cardiac cycle, described by the Bernoulli equation. We assume unsteady, incompressible and non-viscous laminar flow. We assume that no pressure is regained after the valve despite the velocity decrease, representing energy lost through friction or turbulence. In simulations of MR or TR, a "closed" valve has an effective regurgitant orifice (ERO) allowing backflow **(Supplementary Figure 2)**.

### FIBRE STRESS

A phenomenological model describes the dynamic relationship between myofibre stress and strain and determines cavity pressure by Laplace's law[14,15]. The active stress component incorporates length dependence of the force generated and the duration of contraction **(Supplementary Appendix 1)**.

### BASELINE SIMULATIONS

For all simulations, the opening areas of the mitral and tricuspid valves were set to 6 cm², and the aortic and pulmonary valves were set to 3.5 cm². We started with a healthy reference simulation[15]. The ERO area was set to 0.3 cm² in the mitral or tricuspid valve to simulate compensated MR or TR, respectively. Using homeostatic control, CO was maintained at 5.1 l/min and MAP was maintained at 90 mmHg with a heart rate of 70 bpm. We then simulated tissue adaptation in response to chronic regurgitation, as

described previously[19]. The resulting simulations represent a compensated and well-tolerated mild regurgitation.

### DECOMPENSATED REGURGITATION

Decompensated mitral or tricuspid regurgitation is simulated by taking the compensated MR or TR simulations and increasing the ERO area to 0.5 $cm^2$ and 0.7 $cm^2$ in the mitral or tricuspid valve. Heart rate is maintained at 70 bpm but, to represent the compromised haemodynamic status of patients with decompensated regurgitation requiring surgery, CO is reduced to 3.6 l/min and MAP to 75 mmHg.

### MYOCARDIAL DYSFUNCTION

To represent myocardial failure following decompensation, we simulated varying degrees of myocardial dysfunction on the left and/or right side of the heart. On the left side, the left ventricular (LV) free wall, septum, and left atrial (LA) myocardium were dysfunctional, and on the right side the right ventricular (RV) free wall and right atrial (RA) myocardium were made dysfunctional. Both atria and ventricles were affected because chronic regurgitation is associated with atrial remodelling[20,21]. Myocardial dysfunction was simulated by replacing 0-40% of the wall volume with non-contractile fibrotic tissue with 3× the stiffness of healthy myocardium. Haemodynamics were stabilised by homeostatic control.

### PULMONARY HYPERTENSION

TR commonly occurs secondarily to pulmonary hypertension (PH)[22]. We therefore repeated all TR simulations with PH present by tripling the resistance of the pulmonary circulation **(Supplementary Appendix 1)**.

### ABRUPT AND GRADUAL CORRECTION OF REGURGITATION

Abrupt correction of regurgitation was simulated by setting the ERO area of the mitral or tricuspid valve to zero once a cardiac cycle completed. Gradual closure was simulated by reducing the ERO area by 0.03 $cm^2$ per homeostatic control cycle until it reached zero **(Figure 2B)**. In both cases, homeostatic control remained active and gradually altered systemic vascular resistance and blood volume to return to the same CO and MAP as before the intervention. Each simulation ran for 30 homeostatic control cycles to allow haemodynamic stabilisation. The maximum myofibre stress in each simulation cycle was used to quantify the change in myocardial load following correction of MR or TR.

## Results

### BASELINE SIMULATIONS OF MR AND TR

Haemodynamics at baseline are shown in **Figure 3**. Backflow occurs across the mitral valve during LV systole in the simulations with MR. Forward flow across the mitral valve during LV diastole is also increased, as shown by increased E- and A-wave magnitude. The retrograde flow with MR increases with ERO area (**Figure 3A**, top left). Pressure-volume loops show loss of LV isovolumetric contraction and relaxation phases in the simulations with MR (**Figure 3A**, centre). Filling pressures are not increased in the compensated MR simulation but are increased in the decompensated simulations. The simulation with reduced LV and LA myocardial function also has LV dilation (**Figure 3A**, centre) and increased RV systolic pressure secondary to LV failure (**Figure 3A**, right).

In the TR simulations, backflow occurs across the tricuspid valve during RV systole (**Figure 3B**, bottom left), causing RV dilation loss of RV isovolumetric contraction and relaxation (**Figure 3B**, right). In the simulations with RV and RA myocardial dysfunction, RV filling pressures increase (**Figure 3B**, right), and RV dilation becomes more pronounced. PH further dilates the RV, causing LV compression. Baseline characteristics are shown in **Supplementary Table 1**. LV ejection fraction (EF) and RVEF remain high in the MR and TR simulations, respectively, even when myocardial dysfunction is present.

### HAEMODYNAMIC ALTERATIONS FOLLOWING CORRECTION OF REGURGITATION

Dramatic changes in LV pressure-volume loop morphology occur immediately after abrupt correction of MR **(Figure 4A)**, with a pronounced increase in ventricular work (loop area) and a spike in peak LV systolic pressure from 102 mmHg to 135 mmHg. A reduction in ventricular work then occurs rapidly (red dashed lines). In contrast, gradual closure of the RO leads to a gradual transition in pressure-volume loop morphology and gradual reduction in ventricular work **(Figure 4B)**. Both simulations reach the same endpoint (solid red lines). Similar behaviour is observed in RV pressure-volume loop morphology following closure of the regurgitant tricuspid valve **(Supplementary Figure 3)**.

A summary of characteristics following haemodynamic stabilisation after correction of MR or TR is shown in **Supplementary Table 2**. EF decreases after repair of regurgitation. Following correction of MR, LVEF decreases from 54% to 26% in the decompensated simulations with 0.7 $cm^2$ ERO area at baseline and 40% LV and RV myocardial dysfunction. In the equivalent simulations with TR, the RVEF decreased from 46% to 29% following correction.

### INFLUENCE OF REGURGITATION SEVERITY ON VENTRICULAR STRESS

Abrupt closure of a regurgitant valve causes a spike in LV and RV fibre stress, as shown in **Figure 5**. The magnitude of the increase in fibre stress depends on the severity of regurgitation prior to intervention. **Figure 5A** shows LV and RV peak fibre stresses for each simulation cycle following abrupt correction of MR with an ERO area at baseline of 0.7 $cm^2$ (black dots). LV fibre stress peaks at 71.7 kPa following abrupt correction. There is a larger increase in LV and RV fibre stresses immediately following abrupt correction of MR with the larger ERO area at baseline (**Figure 6**, left). LV fibre stress increases by 20.5 kPa (40%) with ERO area 0.7 $cm^2$ at baseline as compared to 14.5 kPa (29.7%) with ERO area 0.5 $cm^2$ immediately after abrupt closure, while RV fibre stress increases by 3.6 kPa (14.8%) as compared to 1.9 kPa (8.1%). Gradual correction of MR

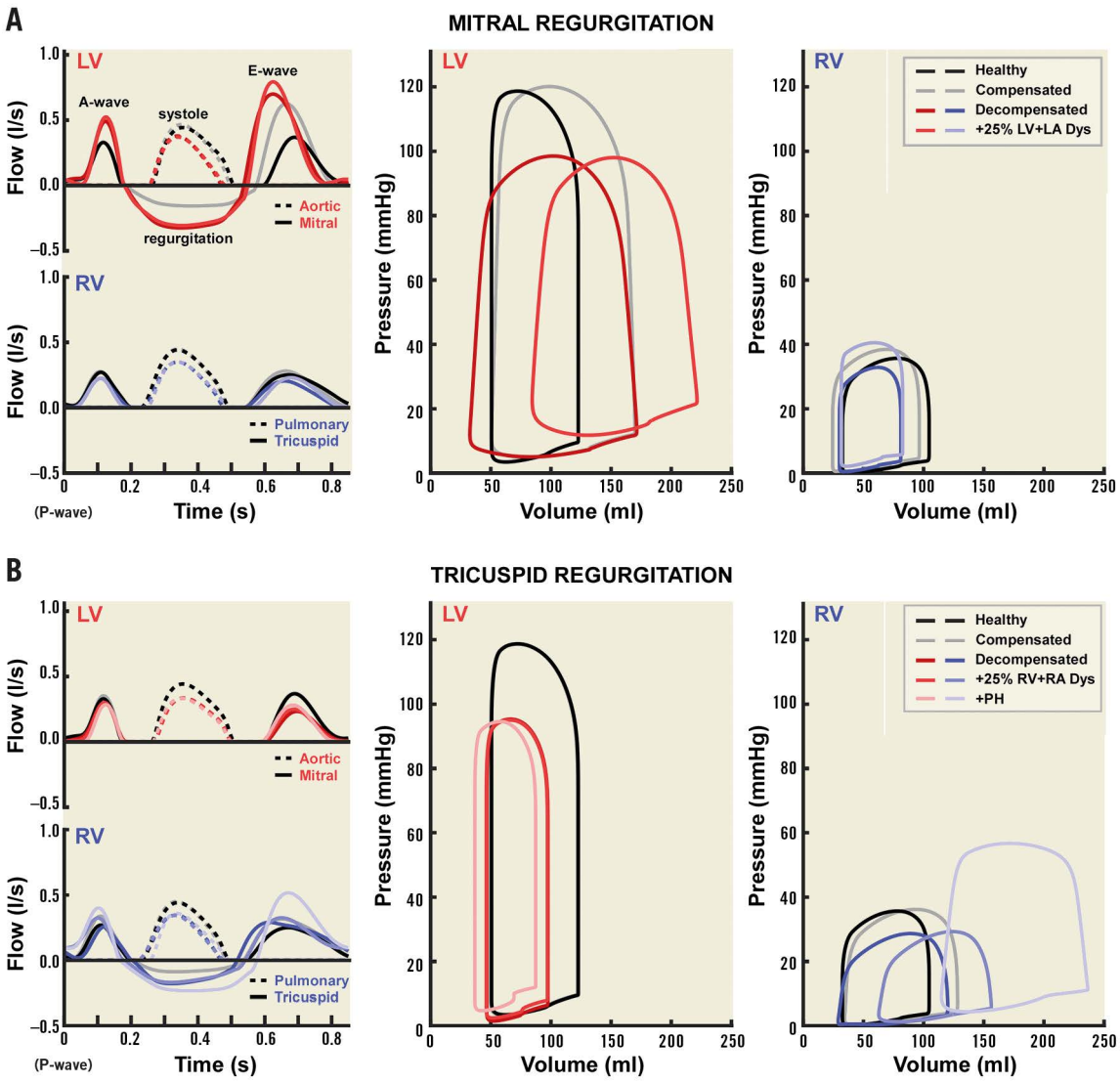


**Figure 3.** *Baseline haemodynamics. Ventricular haemodynamics at baseline are shown for mitral regurgitation (A) and tricuspid regurgitation (B). The left panels show flow patterns across the aortic and mitral valves (top) and pulmonary and tricuspid valves (bottom). The remaining panels show pressure-volume loops for the LV (centre) and RV (right). The healthy (black) and compensated (grey) simulations are shown in all panels. Panel A also shows the 0.7 cm² ERO area decompensated (dark) and +25% LA and LV myocardial dysfunction (light) simulations. Panel B also shows the 0.7 cm² ERO area decompensated (dark), decompensated with 25% RA and RV myocardial dysfunction (medium), and PH with 25% RA and RV myocardial dysfunction (light) simulations.*

abolishes the sudden spike in LV and RV fibre stress (**Figure 5A**, white dots), increasing LV and RV fibre stress by a maximum of 2.4 kPa (4.6%) and 0.4 kPa (1.6%), respectively (**Figure 6**, left).

Abrupt correction of TR leads to sharp increases in both LV and RV fibre stress that are abolished with gradual correction. However, the effects of correction of TR on ventricular stresses are less pronounced than those observed for MR **(Figure 5B)**. As with correction of MR, a larger baseline regurgitation caused a greater increase in LV and RV fibre stress (**Figure 6**, right). Increased RV fibre stress immediately after correction accompanies a slight decrease in LV stress **(Figure 5B)**. Redistribution of blood from left to right subsequently leads to an increase in LV fibre stress. In the simulations with 0.7 cm² ERO area at baseline, sudden closure causes an increase in RV fibre stress of 4.5 kPa (19.5%), as compared with an increase of 3.2 kPa (14.4%) with 0.5 cm² at baseline (**Figure 6**, right). The increase in peak RV fibre stresses with gradual closure was minor (<0.5 kPa, <2%).

PH increases RV maximum fibre stress prior to correction of TR **(Figure 5C)**. The relative change in fibre stress after correction is similar (19.2%) to the non-PH case (**Figure 6A**, right). However, because of the increased RV fibre stress at baseline, the amplitude of the fibre stress spike following sudden correction of TR increases when PH is present, up to 9.2 kPa with an ERO area of 0.7 cm² at baseline (**Figure 6B**, right).

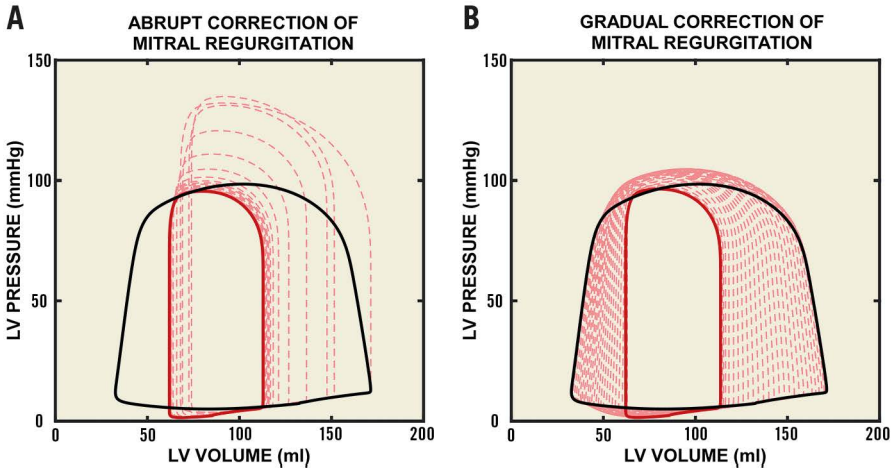


**Figure 4.** *Effect of correction of mitral regurgitation on LV pressure-volume relationships. A) The effect of sudden closure of the ERO in the mitral valve. B) The effect of gradual closure of the ERO. The baseline pressure-volume loop is shown in black with an ERO area of 0.7 cm². The pressure-volume loop after closure and haemodynamic stabilisation is shown in red (solid line). Intermediate pressure-volume loops are also shown (dashed lines).*

## INFLUENCE OF MYOCARDIAL DYSFUNCTION ON VENTRICULAR STRESS

**Supplementary Figure 4** shows the influence of myocardial dysfunction on peak systolic fibre stress following correction of MR and TR. The spike in LV peak systolic stress is present in all simulations with sudden correction of MR but is absent in the gradual closure simulations. In simulations with more extensive myocardial dysfunction, the spike in systolic stress is lower but longer lasting than in simulations with healthier myocardium (**Supplementary Figure 4A**, left). RV peak fibre stress increases more dramatically with myocardial dysfunction than LV peak fibre stress **(Supplementary Figure 4B)**. This elevated peak stress is still present, although lower, after correction of MR. A small spike in RV peak fibre stress is present in all simulations with sudden correction of MR (**Supplementary Figure 4B**, left), and is absent in the gradual correction of MR simulations (**Supplementary Figure 4B**, right). Sudden and gradual corrections of TR with myocardial dysfunction are qualitatively similar to corrections of MR. A more sudden spike in RV systolic fibre stress is observed after correction of TR than MR. A slight dip followed by a sharp rise in LV peak systolic fibre stress occurs following sudden correction of TR, and both are abolished by gradual correction.

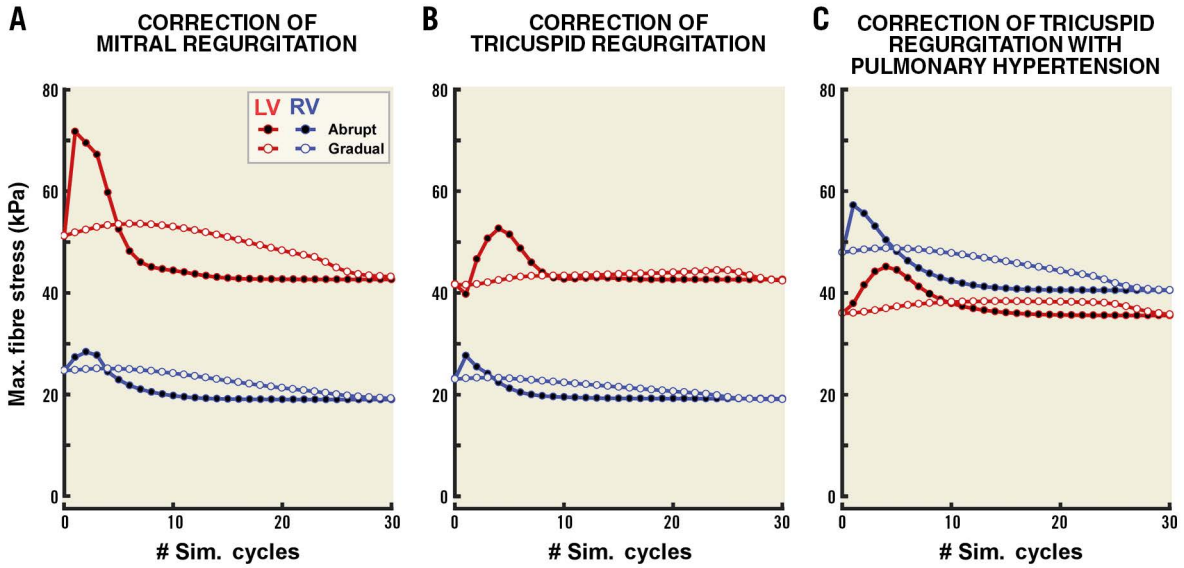


**Figure 5.** *Effect of regurgitation severity and pulmonary hypertension on fibre stress following correction of regurgitation. The time course of LV (red) and RV (blue) peak fibre stress following correction is shown for MR (A), TR (B) and TR with PH (C). ERO area was 0.7 cm² at baseline. Black dots indicate sudden correction and white dots indicate gradual correction.*

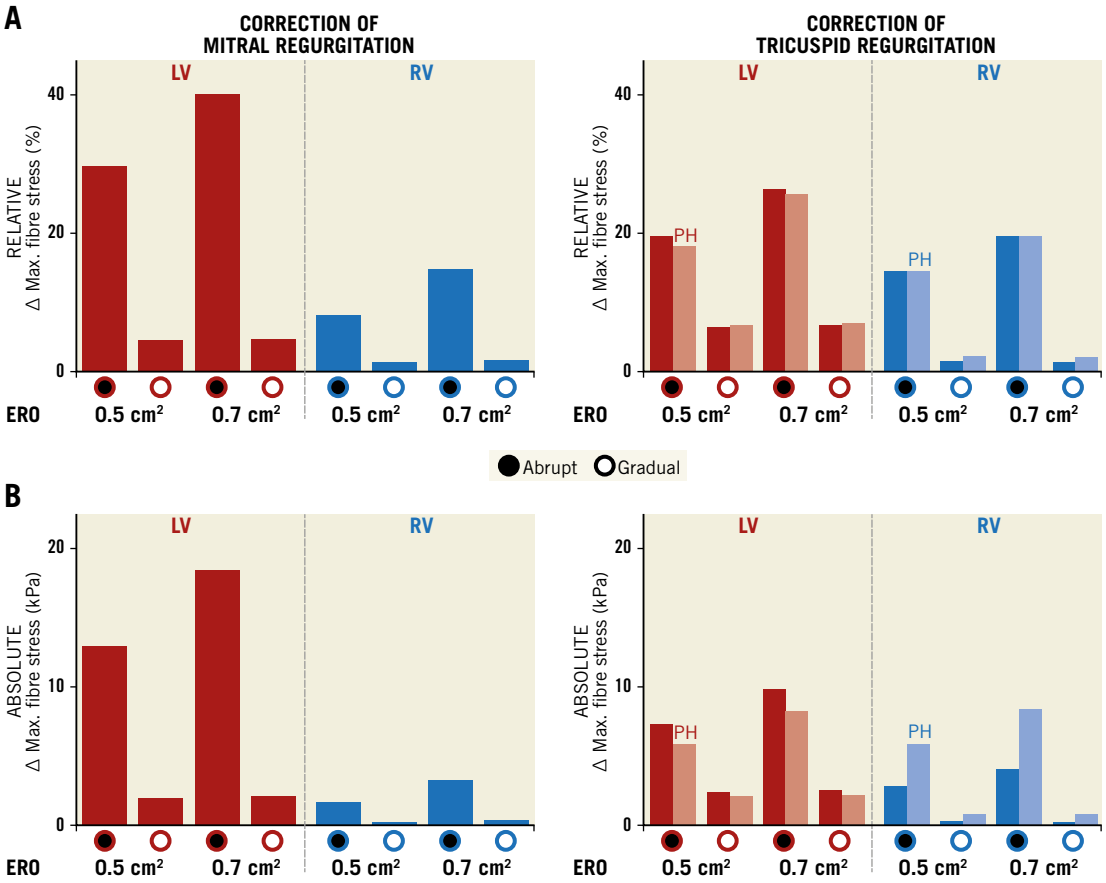


**Figure 6.** *Severity of regurgitation affects fibre stress following correction of regurgitation. A) The maximum percentage change in fibre stress from baseline following correction for the simulations with 0.5 cm² and 0.7 cm² ERO area at baseline. The effect of PH is also shown for tricuspid regurgitation (lighter bars). B) The same data as absolute values.*

## Discussion

The main findings of this simulation study are that: i) abrupt cessation of MR or TR causes a sudden increase in ventricular myocardial stress, and ii) this increase in stress is preventable by gradual reduction of regurgitation. Our findings suggest that acute alterations in ventricular loading may contribute to post-procedural contractile dysfunction in patients following replacement of the mitral and tricuspid valves. Hence, valvular replacement should be adapted to achieve gradual termination of regurgitation.

Earlier studies demonstrated that mitral valve surgery can induce LV dysfunction[23-25]. Apparent induction of LV dysfunction following surgery partially reflects the inadequacies of EF as a measure of cardiac function in the presence of regurgitation[26]. EF is by definition higher when regurgitation occurs due to the additional backflow into the atrium increasing the apparent stroke volume. Our study shows a decrease in LVEF or RVEF following termination of mitral or tricuspid regurgitation, respectively, as this backflow is abolished. However, our results also show that an abrupt termination of this backflow causes a sudden increase in myocardial stress. Apparent ventricular dysfunction after surgery may therefore be explained by unmasking of impaired myocardial function that was hidden by regurgitation. However, the association between post-procedural dysfunction and mortality suggests that dysfunction may also result from intervention[25].

Clinical data on wall stress following mitral valve surgery are limited. An acute increase in end-systolic wall stress has been reported in patients during MitraClip® (Abbott Vascular, Santa Clara, CA, USA) implantation procedures, despite decreases in end-diastolic wall stress[27]. An acute increase in systolic pressure was also observed. An earlier study on mitral valve replacement also showed increased end-systolic stress in patients who had chordae tendineae transected during surgery, but not in those with chordal sparing[28]. Our results suggest that these increases in systolic stress are caused by sudden termination of regurgitation.

Myocardial gene expression alters in response to chronic alterations in ventricular load that accompany chronic regurgitation[2]. Furthermore, atrial volume overload leads to atrial enlargement, fibrosis, and fibrillation[20,21]. While simulations cannot represent the full complexity of remodelling in chronic MR and TR, remodelling occurs gradually over a period of weeks, months, or even years in asymptomatic patients[29]. In contrast, current strategies for

repair or replacement immediately alter ventricular loading[27,28]. Consequently, in severely remodelled myocardium, the abrupt change in volume load may cause additional dysfunction even after the initial spike in fibre stress, as the changes in volume loading may be too great for physiological remodelling processes to compensate in the short term. This is of particular importance in transcatheter valve replacement procedures where transient ventricular assistance is not possible.

Chronic ischaemic MR has significant mortality and morbidity following valvular surgery, and there is currently little evidence of a survival benefit from reducing secondary MR[30]. Patients with dilated ventricles and a disproportionate degree of secondary MR may benefit from intervention. Simulations showed that the course of LV tissue load after abrupt correction of MR or TR depends on the severity of global contractile dysfunction, with a lower but prolonged increase in peak tissue stress when myocardial contractile function was impaired. The load increase was greater in simulations with a larger ERO area. This finding may be explained by the decreased ability of "failing" myocardium to contract forcefully enough to cope with increases in ventricular load. Whether these results also apply to hearts with regional myocardial dysfunction (e.g., due to ischaemic heart disease) remains unknown and requires further research. It has been suggested that a benefit of repair over replacement may be, paradoxically, that residual regurgitation is more common following repair of ischaemic mitral regurgitation, reducing the short-term impact of surgery on the heart[31]. Our results support this hypothesis by demonstrating that abrupt termination of regurgitation imposes large increases in stress on the heart, which may be reduced by a persistent regurgitation. However, residual regurgitation following valve replacement is associated with worse long-term outcomes[10]. Our finding supports a gradual approach to complete closure, combining short-term and long-term benefits.

The amplitude of the stress increase after sudden correction of TR was exacerbated by the presence of PH, a common cause of TR[22]. Since correction of TR increased LV fibre stress, a gradual approach to correction of TR concomitant with MR can reduce the impact on both ventricles. A gradual approach to tricuspid replacement may be particularly beneficial when RV afterload is elevated due to conditions such as chronic obstructive pulmonary disorder or pulmonary arterial hypertension. Since PH exacerbated the spike in ventricular load, afterload reduction could also have a role in limiting the impact of abrupt termination of regurgitation on both the LV and the RV.

## Limitations

Although only clinical studies can capture the complexity of a real intervention in patients, computational models allow understanding of basic pathophysiological mechanisms under tightly controlled conditions that are not possible in the clinic. Creating such conditions in animal models is expensive, raises ethical issues, and does not guarantee generalisability to humans. Hence, we established the validity of our concept *in silico*. Homeostatic control in CircAdapt is phenomenological. The thirty cycles shown represent a process occurring over hours or days in humans, meaning that the time for gradual closure should last well beyond the replacement procedure itself. A more complex regulation model is required to determine how quickly the regurgitant orifice should be closed. Although our findings are applicable to surgical valve replacement, our simulations best represent off-pump transcatheter valve replacement, which is feasible in high-risk severe MR patients not eligible for surgery[32]. The transcatheter approach might benefit more from the presented concept because the interventions available to maintain cardiac function during and immediately post procedure are more limited than for surgical approaches.

## Conclusions

Simulations demonstrated that correcting MR or TR causes a spike in ventricular stress that may exacerbate postoperative cardiac dysfunction and explain the need for post-procedural inotropic support. By avoiding dramatic increases in ventricular stress, gradual correction reduces ventricular overload and may allow gradual reverse remodelling to occur. Our *in silico* proof-of-principle study supports designing future transcatheter prosthetic valves to allow gradual correction of regurgitation.

## Impact on daily practice

Current interventions to correct MR or TR are likely to cause a large transient increase in ventricular load that may be harmful in the short term, despite their longer-term benefits, explaining the relatively challenging course of these patients in the days after the procedure. Future transcatheter interventions for valve replacement may therefore allow a gradual reduction of regurgitation that prevents sudden alterations in ventricular loading and allows a more gradual reverse remodelling to occur.

## Conflict of interest statement

J. Lumens and J. Walmsley report research grants from Medtronic plc. R. Cornelussen and U. Wolfhard are Medtronic plc employees. R. Cornelussen and U. Wolfhard are co-inventors on patents related to the concept. P. Squara reports funding from Medtronic plc for patent maintenance fees. J. Walmsley & J. Lumens: consultancy fees from Medtronic plc.

## References

1. Agricola E, D'Amato R, Stella S, Oppizzi M, Slavich M, Ancona MB, Gullace M, Margonato A. Effects of mild ischemic mitral regurgitation on ventricular remodeling and its contribution to congestive heart failure. *J Am Soc Echocardiogr.* 2011;24:1376-82.

2. Pu M, Gao Z, Zhang X, Liao D, Pu DK, Brennan T, Davidson WR Jr. Impact of mitral regurgitation on left ventricular anatomic and molecular remodeling and systolic function: implication for outcome. *Am J Physiol Circ Physiol.* 2009;296:H1727-32.

3. Kehat I, Molkentin JD. Molecular pathways underlying cardiac remodeling during pathophysiological stimulation. *Circulation.* 2010;122:2727-35.

4. Russell B, Motlagh D, Ashley WW. Form follows function: how muscle shape is regulated by work. *J Appl Physiol.* 2000;88:1127-32.

5. Naji P, Griffin BP, Barr T, Asfahan F, Gillinov AM, Grimm RA, Rodriguez LL, Mihaljevic T, Stewart WJ, Desai MY. Importance of exercise capacity in predicting outcomes and determining optimal timing of surgery in significant primary mitral regurgitation. *J Am Heart Assoc.* 2014;3:e001010.

6. Nishimura RA, Otto CM, Bonow RO, Carabello BA, Erwin JP 3rd, Fleisher LA, Jneid H, Mack MJ, McLeod CJ, O'Gara PT, Rigolin VH, Sundt TM 3rd, Thompson A. 2017 AHA/ACC Focused Update of the 2014 AHA/ACC Guideline for the Management of Patients With Valvular Heart Disease: A Report of the American College of Cardiology/American Heart Association Task Force on Clinical Practice Guidelines. *J Am Coll Cardiol.* 2017;70:252-89.

7. Chikwe J, Itagaki S, Anyanwu A, Adams DH. Impact of Concomitant Tricuspid Annuloplasty on Tricuspid Regurgitation, Right Ventricular Function, and Pulmonary Artery Hypertension After Repair of Mitral Valve Prolapse. *J Am Coll Cardiol.* 2015;65:1931-8.

8. Cho IJ, Moon J, Shim CY, Jang Y, Chung N, Chang BC, Ha JW. Different clinical outcome of paravalvular leakage after aortic or mitral valve replacement. *Am J Cardiol.* 2011;107:280-4.

9. Suri RM, Clavel MA, Schaff HV, Michelena HI, Huebner M, Nishimura RA, Enriquez-Sarano M. Effect of Recurrent Mitral Regurgitation Following Degenerative Mitral Valve Repair: Long-Term Analysis of Competing Outcomes. *J Am Coll Cardiol.* 2016;67:488-98.

10. Edwards FH, Peterson ED, Coombs LP, DeLong ER, Jamieson WR, Shroyer ALW, Grover FL. Prediction of operative mortality after valve replacement surgery. *J Am Coll Cardiol.* 2001;37:885-92.

11. Beckmann A, Funkat AK, Lewandowski J, Frie M, Ernst M, Hekmat K, Schiller W, Gummert JF, Harringer W. German Heart Surgery Report 2016: The Annual Updated Registry of the German Society for Thoracic and Cardiovascular Surgery. *Thorac Cardiovasc Surg.* 2017;65:505-18.

12. Udesh R, Mehta A, Gleason TG, Wechsler L, Thirumala PD. Perioperative Strokes and Early Outcomes in Mitral Valve Surgery: A Nationwide Analysis. *J Cardiothorac Vasc Anesth.* 2017;31:529-36.

13. Arts T, Delhaas T, Bovendeerd P, Verbeek X, Prinzen FW. Adaptation to mechanical load determines shape and properties of heart and circulation: the CircAdapt model. *Am J Physiol Heart Circ Physiol.* 2005;288:H1943-54.

14. Lumens J, Delhaas T, Kirn B, Arts T. Three-wall segment (TriSeg) model describing mechanics and hemodynamics of ventricular interaction. *Ann Biomed Eng.* 2009;37:2234-55.

15. Walmsley J, Arts T, Derval N, Bordachar P, Cochet H, Ploux S, Prinzen FW, Delhaas T, Lumens J. Fast Simulation of Mechanical Heterogeneity in the Electrically Asynchronous Heart Using the MultiPatch Module. *PLoS Comput Biol.* 2015;11:e1004284.

16. Palau-Caballero G, Walmsley J, Gorcsan J 3rd, Lumens J, Delhaas T. Abnormal Ventricular and Aortic Wall Properties Can Cause Inconsistencies in Grading Aortic Regurgitation Severity: A Computer Simulation Study. *J Am Soc Echocardiogr.* 2016;29:1122-30.

17. Lumens J, Arts T, Marcus JT, Vonk-Noordegraaf A, Delhaas T. Early-diastolic left ventricular lengthening implies pulmonary hypertension-induced right ventricular decompensation. *Cardiovasc Res.* 2012;96:286-95.

18. Leenders GE, Lumens J, Cramer MJ, De Boeck BW, Doevendans PA, Delhaas T, Prinzen FW. Septal deformation patterns delineate mechanical dyssynchrony and regional differences in contractility: analysis of patient data using a computer model. *Circ Heart Fail.* 2012;5:87-96.

19. Arts T, Lumens J, Kroon W, Delhaas T. Control of whole heart geometry by intramyocardial mechano-feedback: a model study. *PLoS Comput Biol.* 2012;8:e1002369.

20. Foglieni C, Rusconi R, Mantione ME, Fragasso G, Alfieri O, Maisano F. Early left atrial tissue features in patients with chronic mitral regurgitation and sinus rhythm: Alterations of not remodeled left atria. *Int J Cardiol.* 2016;219:433-8.

21. Nemoto N, Lesser JR, Pedersen WR, Sorajja P, Spinner E, Garberich RF, Vock DM, Schwartz RS. Pathogenic structural heart changes in early tricuspid regurgitation. *J Thorac Cardiovasc Surg.* 2015;150:323-30.

22. Dreyfus GD, Martin RP, Chan KM, Dulguerov F, Alexandrescu C. Functional tricuspid regurgitation: a need to revise our understanding. *J Am Coll Cardiol.* 2015;65:2331-6.

23. Enriquez-Sarano M, Tajik AJ, Schaff HV, Orszulak TA, McGoon MD, Bailey KR, Frye RL. Echocardiographic prediction of left ventricular function after correction of mitral regurgitation: results and clinical implications. *J Am Coll Cardiol.* 1994;24:1536-43.

24. Matsumura T, Ohtaki E, Tanaka K, Misu K, Tobaru T, Asano R, Nagayama M, Kitahara K, Umemura J, Sumiyoshi T, Kasegawa H, Hosoda S. Echocardiographic prediction of left ventricular dysfunction after mitral valve repair for mitral regurgitation as an indicator to decide the optimal timing of repair. *J Am Coll Cardiol.* 2003;42:458-63.

25. Reed D, Abbott RD, Smucker ML, Kaul S. Prediction of outcome after mitral valve replacement in patients with symptomatic chronic mitral regurgitation. The importance of left atrial size. *Circulation.* 1991;84:23-34.

26. Carabello BA. A tragedy of modern cardiology: using ejection fraction to gauge left ventricular function in mitral regurgitation. *Heart.* 2017;103:570-1.

27. Gaemperli O, Biaggi P, Gugelmann R, Osranek M, Schreuder JJ, Buhler I, Surder D, Luscher TF, Felix C, Bettex D, Grunenfelder J, Corti R. Real-time left ventricular pressure-volume loops during percutaneous mitral valve repair with the MitraClip system. *Circulation.* 2013;127:1018-27.

28. Rozich JD, Carabello BA, Usher BW, Kratz JM, Bell AE, Zile MR. Mitral valve replacement with and without chordal preservation in patients with chronic mitral regurgitation. Mechanisms for differences in postoperative ejection performance. *Circulation.* 1992;86:1718-26.

29. Neilan TG, Ton-Nu TT, Kawase Y, Yoneyama R, Hoshino K, del Monte F, Hajjar RJ, Picard MH, Levine RA, Hung J. Progressive nature of chronic mitral regurgitation and the role of tissue Doppler-derived indexes. *Am J Physiol Circ Physiol.* 2008;294:H2106-11.

30. Baumgartner H, Falk V, Bax JJ, De Bonis M, Hamm C, Holm PJ, Iung B, Lancellotti P, Lansac E, Rodriguez Munoz D, Rosenhek R, Sjogren J, Tornos Mas P, Vahanian A, Walther T, Wendler O, Windecker S, Zamorano JL; ESC Scientific Document Group. 2017 ESC/EACTS Guidelines for the management of valvular heart disease. *Eur Heart J.* 2017;38:2739-91.

31. Vural KM. Why Does Prosthetic Replacement Seemingly Have Higher Perioperative Mortality Than Valve Repair in Ischemic Mitral Regurgitation? *Thorac Cardiovasc Surg.* 2017;65:445-6.

32. Webb JG, Murdoch DJ, Boone RH, Moss R, Attinger-Toller A, Blanke P, Cheung A, Hensey M, Leipsic J, Ong K, Sathananthan J, Wood DA, Ye J, Tartara P. Percutaneous Transcatheter Mitral Valve Replacement: First-in-Human Experience With a New Transseptal System. *J Am Coll Cardiol.* 2019;73:1239-46.

33. Kondo M, Washizu M, Matsukura Y, Washizu T, Miyasaka K, Takata M. Pressure-flow relationship and longitudinal distribution of pulmonary vascular resistance in heartworm-infected dogs. *J Vet Med Sci.* 2003;65:965-70.

34. Arts T, Reesink K, Kroon W, Delhaas T. Simulation of adaptation of blood vessel geometry to flow and pressure: Implications for arterio-venous impedance. *Mech Res Commun.* 2012;42:15-21.

35. Lumens J, Tayal B, Walmsley J, Delgado-Montero A, Huntjens PR, Schwartzman D, Althouse AD, Delhaas T, Prinzen FW, Gorcsan J 3rd. Differentiating Electromechanical From Non-Electrical Substrates of Mechanical Discoordination to Identify Responders to Cardiac Resynchronization Therapy. *Circ Cardiovasc Imaging.* 2015;8:e003744.

36. de Tombe PP, ter Keurs HE. Force and velocity of sarcomere shortening in trabeculae from rat heart. Effects of temperature. *Circ Res.* 1990;66:1239-54.

37. ter Keurs HE, Rijnsburger WH, van Heuningen R, Nagelsmit MJ. Tension development and sarcomere length in rat cardiac trabeculae. Evidence of length-dependent activation. *Circ Res.* 1980;46:703-14.

## Supplementary data

**Supplementary Appendix 1.** Methods.

**Supplementary Figure 1.** Flow chart showing how the simulations used in each Figure in the main article are constructed.

**Supplementary Figure 2.** Definitions used in the text for the simulation of valvular function.

**Supplementary Figure 3.** Effect of correction of tricuspid regurgitation on RV pressure-volume relationships.

**Supplementary Figure 4.** Effect of myocardial dysfunction on fibre stress following correction of regurgitation.

**Supplementary Table 1.** Baseline characteristics.

**Supplementary Table 2.** Post-correction characteristics.

*The supplementary data are published online at: https://eurointervention.pcronline.com/doi/10.4244/EIJ-D-19-00598*

**Supplementary data**

**Supplementary Appendix 1. Methods**

**Flow across the systemic and pulmonary circulations**

The CircAdapt model consists of a four-chamber heart connected to a closed loop cardiovascular system, with lumped pulmonary and systemic circulations. The systemic circulation is modelled as a vascular resistance connecting the aorta with the systemic veins. In CircAdapt, both the arterial and venous pressures vary with time, and the pressure difference between the arteries and veins determines the flow across the systemic circulation at any point in time, *t*. The time-dependent flow across the systemic circulation $q_{sys}(t)$ is assumed to relate with time-dependent pressure drop $\Delta p_{sys}(\mathrm{t})$ as,

$$q_{sys}(t) = \frac{q_{sys,ref}}{\Delta p_{sys,ref}} \cdot \Delta p_{sys}(\mathrm{t}) \quad (1)$$

where $q_{sys,ref}$ is the reference circulating blood flow and $\Delta p_{sys,ref}$ is the corresponding reference systemic pressure drop. $\Delta p_{sys}(\mathrm{t}) = p_{sys,art}(t) - p_{sys,ven}(t)$ is the difference between the pressure in the systemic arteries ($p_{sys,art}(t)$) and the systemic veins ( $p_{sys,ven}(t)$ ) at each time point. By Ohm's law, $\frac{q_{sys,ref}}{\Delta p_{sys,ref}}$ is the resistance of the systemic vasculature. In the CircAdapt model, $q_{sys,ref}$ is always held constant, but $\Delta p_{sys,ref}$ can be changed between cardiac cycles in the homeostatic control system described below. Hence, changing $\Delta p_{sys,ref}$ changes the systemic resistance in CircAdapt. Intuitively, $\Delta p_{sys,ref}$ can be seen as the pressure difference between the systemic arteries and systemic veins that would be required to generate a constant systemic flow of $q_{sys,ref}$. The relationship for the pulmonary circulation is similar to **Eq. 1**,

$$q_{pulm}(t) = \frac{q_{pulm,ref}}{\Delta p_{pulm,ref}^2} \cdot \Delta p_{pulm}(t)^2 \quad (2)$$

where $q_{pulm,ref}$ is the reference pulmonary circulating blood flow and $\Delta p_{pulm,ref}$ is the corresponding pulmonary pressure drop. To simulate PH in this study, we tripled $\Delta p_{pulm,ref}$. The quadratic relationship in **Eq. 2** is based on measurements of pulmonary circulatory haemodynamics in dogs [33]. A description of the systemic and pulmonary circulation models, including the pressure-volume relationships in the major arteries and veins, is provided by Arts et al (2012) [34].

**Pressure-flow regulation**

In CircAdapt, homeostatic pressure-flow regulation is used to maintain a target cardiac output ($q_{sys,target}$) and target mean systemic arterial pressure ($MAP_{target}$). In the current study, $q_{sys,target}$ changes depending on the level of exercise. Note that $q_{sys,target}$ is not necessarily the same as $q_{sys,ref}$ in **Eq. 1** above. In CircAdapt, homeostatic pressure-flow regulation represents two physiological processes. Acutely, it represents the recruitment of pooled blood in the venous system into the circulating blood volume. In the longer term (for example when employed in simulations of heart failure [35]), it represents the long-term action of the renin-angiotensin-aldosterone system (RAAS) on fluid retention to maintain cardiac output.

When pressure-flow regulation is enabled, CircAdapt calculates at the end of each cardiac cycle the ratio between the current mean systemic arterial pressure over the cardiac cycle ($MAP_{current} = \overline{p_{sys,art}(t)}$) and the target mean aortic pressure ($MAP_{target}$). This ratio is then used to alter the systemic resistance incrementally through changes in $\Delta p_{sys,ref}$ (**Eq. 1**), with the process repeated over repeated cardiac cycles until $MAP_{current} = MAP_{target}$. In this study, a $MAP_{target}$ of 90 mmHg was used. After each cardiac cycle, the new value of the constant $\Delta p_{sys,ref}$, which determines the systemic vascular resistance during the next cardiac cycle (**Eq. 1**), is calculated using:

$$\Delta p_{sys,ref,new} = \left(\frac{MAP_{target}}{MAP_{current}}\right)^{\alpha} \cdot \left(\frac{q_{sys,current}}{q_{sys,target}}\right)^{\alpha} \Delta p_{sys,ref,old} \qquad (3)$$

Hence, the systemic vascular resistance will increase when MAP is too low and decrease when systemic flow is too low. $\alpha<1$ is a damping factor that prevents oscillatory behaviour. Note that the pulmonary resistance remains unchanged by homeostatic control.

To represent RAAS and/or recruitment of pooled blood, the circulating blood volume alters with the systemic vascular resistance. These processes are implemented by injecting or removing volume per cardiac cycle into the cardiac system from the systemic vascular bed, i.e., by altering the flow at the arrow highlighted in **Supplementary Figure 1** (panel A, red arrow). The flow across the systemic circulation $q(t)$ is calculated at each time point $t$ in the cardiac cycle using **Eq. 1**. The flow entering the systemic veins $q_{ven}(t)$ at each time point is then adjusted, so that

$$q_{ven}(t) = \left(\frac{MAP_{target}}{MAP_{current}}\right)^{\alpha} q(t) \qquad (4)$$

Equivalently, **Eq. 4** can be seen as including an additional flow of magnitude $\left(\left(\frac{MAP_{target}}{MAP_{current}}\right)^{\alpha} - 1\right) q(t)$ into the flow exiting the systemic circulation into the systemic veins. Note that if $MAP_{target} > MAP_{current}$, then the additional flow is positive, analogous to recruitment of pooled blood into the circulation or fluid retention by RAAS. If $MAP_{current} > MAP_{target}$ then this flow is negative and removes blood from the circulation, analogous to blood pooling in the veins or fluid excretion through RAAS.

**Valve module and mitral and tricuspid valve regurgitation**

The valve module is used to simulate blood flow across any connection between two cavities or a cavity and a tube in the CircAdapt model where energy losses might occur. Cardiac valves connect cardiac cavities, representing atrioventricular valves, or connect cardiac cavities with large blood vessels, representing ventriculo-arterial valves. The valve module is also used to represent connections between veins and atria, or atrial and ventricular septal defects. The valve module consists of a narrow orifice whose area varies over time during a cardiac cycle. Assuming unsteady, incompressible and non-viscous laminar flow, and the influence of gravity being neglected, the Bernoulli equation for unsteady flow can be written as,

$$I \cdot \frac{dq}{dt} + \frac{1}{2}\rho \cdot \left(v_{dist}(t)^2 - v_{prox}(t)^2\right) + \left(p_{dist}(t) - p_{prox}(t)\right) = 0 \quad (5)$$

where $\rho$ is blood density, $I$ is the inertance of the valve, and $dq/dt$ is the rate of change of blood flow across the valve. The blood flow velocities and pressures at the proximal and distal elements are $v_{prox}(t)$ and $p_{prox}(t)$, and $v_{dist}(t)$ and $p_{dist}(t)$, respectively **(Supplementary Figure 1)**. By re-arranging **Eq. 5**, the pressure gradient ($\Delta p(t) = p_{prox}(t) - p_{dist}$) can be expressed as,

$$\Delta p(t) = I\frac{dq}{dt} + \frac{1}{2}\rho \cdot \left(v_{dist}(t)^2 - v_{prox}(t)^2\right) \quad (6)$$

Since we assume that when blood flow passes a valve, there is no regain in pressure despite a decrease in velocity (i.e., energy is lost by means of friction or turbulence), **Eq. 6** can be re-arranged as,

$$\Delta p(t) = I \cdot \frac{dq_{valve}}{dt} + \frac{1}{2}\rho \cdot \begin{cases} v_{max}(t)^2 - v_{prox}(t)^2, & q_{valve}(t) \geq 0 \\ v_{dist}(t)^2 - v_{max}(t)^2, & q_{valve}(t) < 0 \end{cases} \quad (7)$$

The pressure gradient in **Eq. 7** is the sum of inertial effects, i.e., blood acceleration/deceleration because of blood mass (**Eq. 7**, right-hand side, first term) and

Bernoulli pressure loss effects (**Eq. 7**, right-hand side, second term). Blood flow, $q_{valve}$(t), across a valve is defined as forward flow ($q_{valve}(t) \geq 0$) when it travels from the proximal into the distal element, and backward flow ($q_{valve}(t) < 0$) in the opposite direction. In **Eq. 7**, the maximum velocity, $v_{max}(t)$, is:

$$v_{\max}(t) = max\{v_{prox}(t), v_{valve}(t), v_{dist}(t)\}. \quad (8)$$

Flow velocities $v_{prox}(t)$, $v_{valve}(t)$ and $v_{dist}(t)$ are calculated as valve flow, $q_{valve}(t)$, divided by the cross-sectional area at the proximal element, valve and distal elements at time $t$, respectively. The effective orifice area (or cross-sectional area) of a valve at time $t$, $A_{valve}(t)$, is determined by the pressure gradient. When the valve is open, $A_{valve}(t) = A_{open}$, and, when it is closed, $A_{valve}(t) = A_{leak}$. The valve opens rapidly when the pressure gradient is positive ($p_{dist}(t) < p_{prox}(t)$), allowing forward flow across the valve into the distal element. When the distal pressure is equal to the proximal pressure ($p_{dist}(t) = p_{prox}(t)$), the valve starts closing. In the closing state, the pressure gradient is negative ($p_{dist}(t) > p_{prox}(t)$), but a forward flow can briefly exist because of inertial effects (**Eq. 7**). A valve finally closes when the pressure gradient is negative and no forward flow remains. Note that, in this study, a "closed" valve allows retrograde flow to occur through the regurgitant orifice area as described in the main text, because $A_{leak}$ can be non-zero.

The inertance of a tube $I = \alpha \frac{\rho l}{A}$, where l is the length of the tube and A is the cross-sectional area. $\alpha$ is a constant reflecting the non-linearity of the flow profile. CircAdapt uses $\alpha$=3/2, representing a highly non-linear flow through the valve (compare with $\alpha$=1 for plug flow and $\alpha$=4/3 for Poiseuille flow). In CircAdapt, the inertance takes blood moving through the areas immediately proximal to the valve into account, and immediately distal to the valve **(Supplementary Figure 2)**. Combining these effects gives a total expression for the inertance as

$$I = \frac{3}{2}\rho\left(\frac{l_{valve}}{A_{valve}} + \frac{1}{2}\left(\frac{1}{\sqrt{A_{prox}}} + \frac{1}{\sqrt{A_{dist}}}\right)\right) \quad (9)$$

Note that the valve module is used to connect any two cavities in the CircAdapt model where energy losses might occur, such as veins returning to the atria, or in case of an atrial or ventricular septal defect. In these cases, we define $A_{leak} = A_{open}$.

**Fibre stress model**

The contraction model currently used in CircAdapt is a modified Hill model based upon the one presented by Lumens et al (2009) [14]. The model aims to reproduce basic properties of length-dependent activation in cardiac tissue [36,37]. The fibre stress is determined by the rise of contractility in the fibre (density of cross bridge formation) and the fibre strain. The fibre model is divided into an active and a passive stress component, with the active stress arising from myofibre contraction, and the passive stress component arising from the soft tissue deformation of the myocardium.

The current myofibre strain is used to compute the sarcomere length in the model. In CircAdapt, natural myofibre strain $\varepsilon_f$ in a patch is defined as

$$\varepsilon_f = \ln \frac{L_s}{L_{s,\mathrm{Ref}}}, \tag{10}$$

where $L_s$ is the total sarcomere length, and $L_{s,Ref}$ is the reference sarcomere length of 2 µm. From the strain we can therefore calculate the sarcomere length as

$$L_s = L_{s,\mathrm{ref}} \exp(\varepsilon_f) \tag{11}$$

**Active stress**

The fibre active stress is determined by a modified Hill model controlled by two variables, the intrinsic sarcomere length $L_{si}$ and the contractility $C$. The governing equation for $L_{si}$ is

$$\frac{dL_{si}}{dt} = v_{\max} \left( \frac{L_s - L_{si}}{L_{se,\mathrm{iso}}} - 1 \right), \tag{12}$$

where $L_s - L_{si}$ is the length of the series elastic element in the Hill model, and $L_{se,iso}$ is the length of the series elastic element during isovolumetric contraction. The length of the series elastic element represents the deformation of the sarcomere due to stretch of cross bridges under mechanical load during contraction.

Contractility is a phenomenological parameter representing the density of cross bridge formation within the fibres in the current patch. The contractility is determined by the following differential equation,

$$\frac{dC}{dt} = \frac{1}{\tau_{\text{rise}}} C_L(L_{si})\, F_{\text{rise}}(t) - \frac{1}{\tau_{\text{decay}}} C\ \text{g(X)}. \tag{13}$$

where,

$$\tau_{\text{rise}} = 0.55\, T_r T_{ACT}, \tag{14}$$

$$\tau_{\text{decay}} = 0.33\, T_d T_{ACT}. \tag{15}$$

$T_r$ and $T_d$ are constants, and $T_{ACT}$ is the rate-dependent activation duration. $C_L$ describes the increase in cross bridge formation with intrinsic sarcomere length due to an increase in available binding sites,

$$C_L(L_{si}) = \tanh\left(4\left(L_{si} - L_{si,0}\right)^2\right). \tag{16}$$

$F_{rise}(t)$ is a phenomenological representation of the rate of cross bridge formation within the patch,

$$F_{\text{rise}}(t) = 0.02\, x^3 (8 - x)^2 \exp(-x), \tag{17}$$

where

$$x(t) = \min\left(8, \max\left(0, \frac{t_c}{\tau_{\text{rise}}}\right)\right), \tag{18}$$

and $t_c = t - t_{onset}$, where $t_{onset}$ is the time of onset of activation of the patch, *i.e.*, the time at which the first myocytes within the patch begin to form cross bridges in response to electrical activation.

The decay term in **Eq. 13** gives an exponential decay in the contractility. This decay is delayed by the term $g(X)$. The term $g(X)$ approximates the function $tanh(X)$ using a sine curve to ensure that it takes value 0 or 1 outside of the region where it exhibits a large change,

$$\text{g(X)} = 0.5 + 0.5\ \sin\left(\text{sign}(X)\ \min\left(\frac{\pi}{2}, \text{abs}(X)\right)\right), \tag{19}$$

where,

$$X = \frac{t_c - t_A}{\tau_d}, \tag{20}$$

and $t_A$ depends on the sarcomere extension,

$$t_A = \left(0.65 + 1.057\ \frac{L_{si}}{L_{si,0}}\right) T_{ACT}. \tag{21}$$

The effect of the formulation for contractility is as follows: as the chamber wall is stretched by an expanding volume of blood, the series elastic element ($L_{se}$) lengthens, causing a corresponding lengthening of the contractile element ($L_{si}$). Given an onset of cross bridge formation in response to electrical excitation of parts of the patch at time $t_{act}$, the contractility $C$ begins to rise according to $F_{rise}(t)$. The longer the contractile element $L_{si}$, the greater both the duration of the contractile phase (**Eq. 7**) and the rate of increase in contractility are (**Eq. 16**). Once the duration of activation, $t_A$, is over, the contractility begins to decay exponentially.

We use the following equations to convert contractility and sarcomere length into actively generated fibre stress $\sigma_{f,actT}$ within a patch,

$$\sigma_{f,actT} = \sigma_{f,act} C (L_{si} - L_{si,ref}) \frac{L_{se}}{L_{se,iso}}, \tag{22}$$

where $\sigma_{f,act}$ is a parameter and $L_{se} / L_{se,iso}$ is the extension of the series elastic element. Hence the actively generated fibre stress is determined by the stretching of the myosin heads in response to sarcomere shortening multiplied by the number of cross bridges formed, which is the contractility multiplied by the sarcomere extension from reference ( $C ( L_{si} - L_{si,ref})$ ).

**Passive stress**

Passive deformation of the soft tissue making up the myocardium will also generate stress within the walls, $\sigma_{f,pasT}$. In CircAdapt, this is considered to be a passive stress in the fibres in each patch. This contains two components, the stress arising from the myocytes themselves due to internal structures such as titin anchoring to the Z disc ($\sigma_{f,tit}$), and the stress arising from the extracellular matrix surrounding the myocytes ($\sigma_{f,ECM}$). Hence,

$$\sigma_{f,pasT} = \sigma_{f,tit} + \sigma_{f,ECM}. \tag{23}$$

The extension of the cells for the passive stress calculation $\lambda_{s,pas}$ is done relative to a different reference length $L_{s0,pas}$ as follows,

$$L_{s,pas} = \frac{L_{s0}}{L_{s0,pas}} \exp(e_f). \tag{24}$$

The ECM is modelled as being stiffer than the contribution due to cellular structures such as titin,

$$\sigma_{f,ECM} = 0.0349\, \sigma_{f,pas} \left({\lambda_{s,pas}}^{10} - 1\right), \tag{25}$$

where $\sigma_{f,pas}$ is a parameter.

The passive stress in the patch due to cellular structures such as titin is modelled as being softer than the ECM, and is governed by the following equation

$$\sigma_{f,tit} = 0.01\ \sigma_{f,act}\left({\lambda_{s,pas}}^{k} - 1\right) \tag{26}$$

where the parameter *k* is given by

$$k = \frac{2L_{s,ref}}{dL_{s0,pas}}, \tag{27}$$

and $dL_{s0,pas}$ is a parameter. Using **Eqs. 22** and **23** we then arrive at the following expression for fibre stress within a patch,

$$\sigma_f = \sigma_{f,actT} + \sigma_{f,pasT}. \tag{28}$$

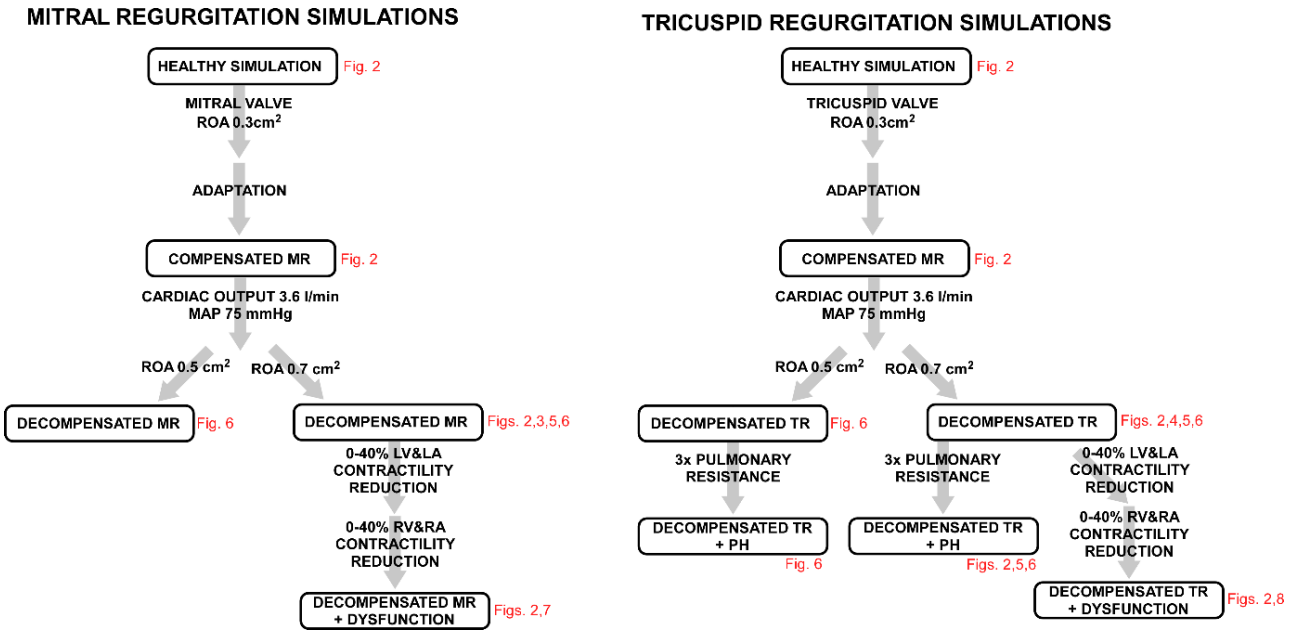


**Supplementary Figure 1.** Flow chart showing how the simulations used in each Figure in the main article are constructed.

Each **DECOMPENSATED** simulation receives both abrupt and gradual closure of the ROA in the mitral or tricuspid valve as appropriate for use in Figures 3-8 in the main article.
LA: left atrium; LV: left ventricle; MAP: mean arterial pressure; MR: mitral regurgitation; PH: pulmonary hypertension; RA: right atrium; ROA: regurgitant orifice area; RV: right ventricle; TR: tricuspid regurgitation

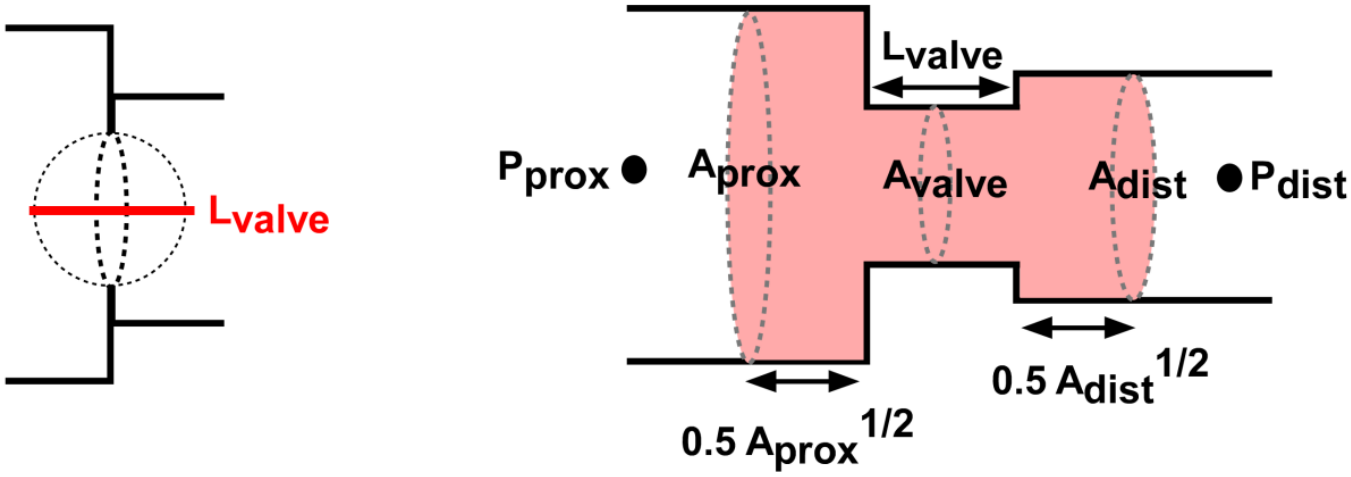


**Supplementary Figure 2.** Definitions used in the text for the simulation of valvular function.

The pink area indicates the total volume of blood considered in the inertance of the valve.

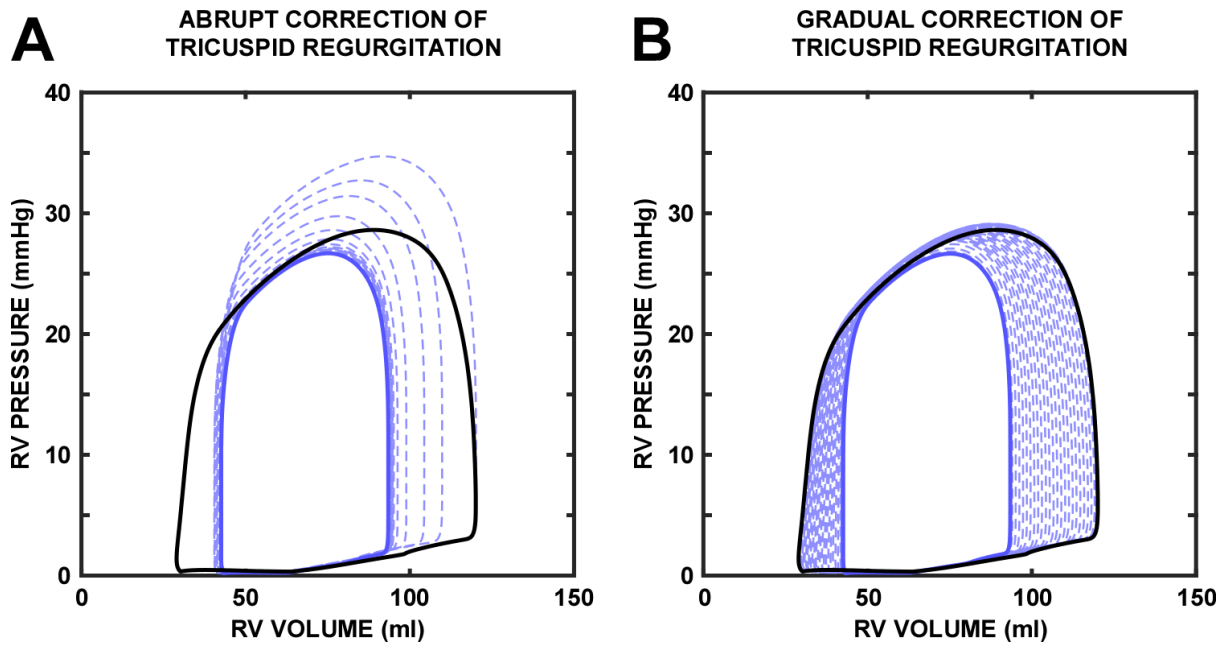


**Supplementary Figure 3.** Effect of correction of tricuspid regurgitation on RV pressure-volume relationships.

A. The effect of abrupt closure of the ROA in the tricuspid valve.

B. The effect of gradual closure. The baseline pressure-volume loop is shown in black with an ROA of 0.7 $cm^2$. The pressure-volume loop after closure and haemodynamic stabilisation is shown in blue (solid line). Intermediate pressure-volume loops are also shown (dashed lines).

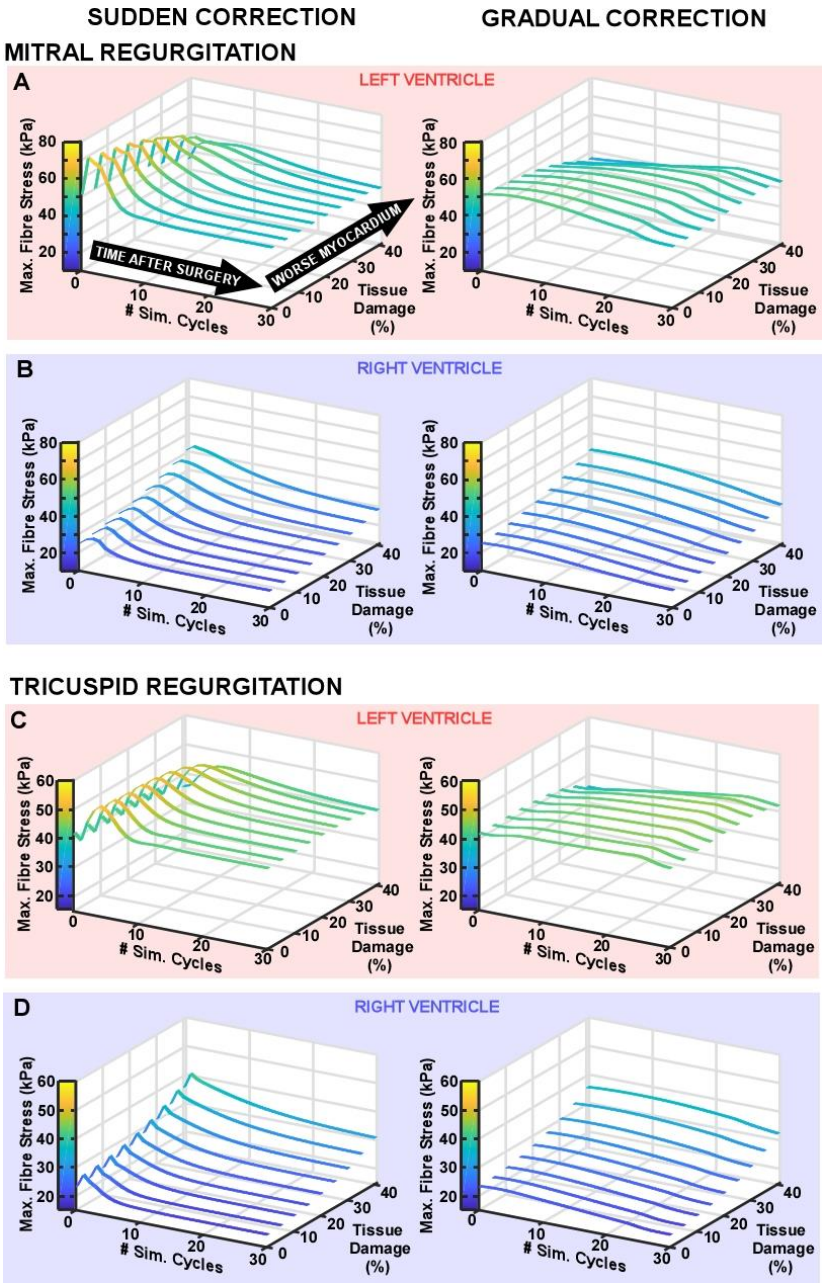


**Supplementary Figure 4.** Effect of myocardial dysfunction on fibre stress following correction of regurgitation.

Results are shown for correction of mitral regurgitation (A, B) and tricuspid regurgitation (C, D). Peak systolic fibre stress in each cycle is shown for the LV (A, C) and RV (B, D). Sudden correction is shown on the left and gradual correction is shown on the right. Simulations with increasing amounts of left- and right-sided myocardial dysfunction are shown going into the page, as indicated by the black arrows in panel A. Both the left and right side of the heart have the same degree of myocardial dysfunction. The colour scale indicates peak fibre stress per cycle.

**Supplementary Table 1. Baseline characteristics.**

| | Normal reference | Compensated MR | Compensated TR | Decompensated MR | Decompensated TR | MR + 40% failure | TR + 40% failure |
|---|---|---|---|---|---|---|---|
| Heart rate (bpm) | 70 | 70 | 70 | 70 | 70 | 70 | 70 |
| Cardiac output (L/min) | 5.1 | 5.1 | 5.1 | 3.6 | 3.6 | 3.6 | 3.6 |
| Mean arterial pressure (mmHg) | 90 | 90 | 90 | 75 | 75 | 75 | 75 |
| Mitral ERO area ($cm^2$) | - | 0.3 | - | 0.7 | - | 0.7 | - |
| Tricuspid ERO area ($cm^2$) | - | - | 0.3 | - | 0.7 | - | 0.7 |
| LV EDV (ml) | 123 | 170 | 122 | 171 | 98 | 231 | 165 |
| LV EF (%) | 59 | 70 | 59 | 81 | 52 | 54 | 31 |
| LV RF (%) | - | 39 | - | 63 | - | 59 | - |
| RV EDV (ml) | 105 | 97 | 128 | 81 | 120 | 194 | 220 |
| RV EF (%) | 69 | 75 | 73 | 63 | 76 | 26 | 46 |
| RV RF (%) | - | - | 23 | - | 44 | - | 50 |

bpm: beats per minute; EDV: end-diastolic volume; EF: ejection fraction; ERO: effective regurgitant orifice; LV: left ventricle; MR: mitral regurgitation; RF: regurgitant fraction; RV: right ventricle; TR: tricuspid regurgitation

**Supplementary Table 2. Post-correction characteristics.**

| | Normal reference | Decompensated MR | Decompensated TR | MR + 40% failure | TR + 40% failure |
|---|---|---|---|---|---|
| Heart rate (bpm) | 70 | 70 | 70 | 70 | 70 |
| Cardiac output (L/min) | 5.1 | 3.6 | 3.6 | 3.6 | 3.6 |
| Mean arterial pressure (mmHg) | 90 | 75 | 75 | 75 | 75 |
| LV EDV (ml) | 123 | 113 | 98 | 200 | 169 |
| LV EF (%) | 59 | 45 | 52 | 26 | 31 |
| RV EDV (ml) | 105 | 75 | 94 | 147 | 178 |
| RV EF (%) | 69 | 68 | 54 | 36 | 29 |

bpm: beats per minute; EDV: end-diastolic volume; EF: ejection fraction; LV: left ventricle; MR: mitral regurgitation; RV: right ventricle; TR: tricuspid regurgitation